Neutron radiative capture cross section of ^{63,65}Cu between 0.4 and 7.5 MeV

I. Newsome, M. Bhike, Krishichayan, and W. Tornow*
Department of Physics, Duke University, Durham, North Carolina 27708, USA
and Triangle Universities Nuclear Laboratory, Durham, North Carolina 27708, USA

(Received 5 December 2017; published 26 April 2018)

Natural copper is commonly used as cooling and shielding medium in detector arrangements designed to search for neutrinoless double-β decay. Neutron-induced background reactions on copper could potentially produce signals that are indistinguishable from the signals of interest. The present work focuses on radiative neutron capture experiments on ^{63,65}Cu in the 0.4 to 7.5 MeV neutron energy range. The new data provide evaluations and model calculations with benchmark data needed to extend their applicability in predicting background rates in neutrinoless double-β decay experiments.

DOI: 10.1103/PhysRevC.97.044617

I. INTRODUCTION

Natural copper is being used as cooling and shielding medium in most searches for neutrinoless double-β ($0\nu\beta\beta$) decay. Here, we refer to the experiments named EXO-200 with its ^{136}Xe-based time projection chamber [1], CUORE using ^{nat}Te compound-based bolometers with focus on ^{130}Te [2], and GERDA [3] and the majorana demonstrator [4], both employing enriched high-purity germanium detectors to search for the $0\nu\beta\beta$ decay of ^{76}Ge. In these experiments, copper is in close contact with the actual detector medium. Although these experiments are performed deep underground, neutron-induced reactions in copper can cause radiation, which potentially could interfere with the signal of interest. Neutrons from muon-induced spallation of nuclei in the surrounding rock and other passive shielding, neutrons from (α,n) reactions initiated by α-particles from the decay of actinide impurities in the detector itself or its shielding, and finally neutrons from fission of ^{238}U can interact with copper nuclei and generate radiation that produces signals which could be indistinguishable from the expected $0\nu\beta\beta$ signal of interest.

The ^{63,65}Cu(n,γ) ^{64,66}Cu radiative capture reactions with Q values of +7916 keV and +7066 keV, respectively, are a potential sources of background. Natural copper consists to 69.2% of ^{63}Cu and to 30.8% of ^{65}Cu. The daughter nucleus ^{64}Cu is unstable and decays with $T_{1/2} = 12.70$ h to either the stable nucleus ^{64}Ni via electron capture (branching ratio of 61.5% and Q value of 1675 keV) or to the stable nucleus ^{64}Zn via β decay (branching ratio of 38.5% and Q value of 579 keV). The daughter nucleus ^{66}Cu is unstable as well and decays with $T_{1/2} = 5.12$ m via β decay and associated Q value of 2641 keV to the stable nucleus ^{66}Zn.

β particle from the decay of ^{66}Cu and de-excitation γ rays from ^{64}Cu and ^{66}Cu could produce signals in the energy windows of interest for $0\nu\beta\beta$ searches, which are centered at 2039 keV for ^{76}Ge, 2458 keV for ^{136}Xe, and 2528 keV for ^{130}Te. Here, we report on ^{63,65}Cu(n,γ) ^{64,66}Cu cross-section measurements in the 0.4 to 7.5 MeV neutron energy range. For the ^{65}Cu(n,γ) ^{66}Cu reaction previous data are lacking for incident neutron energies above 6 MeV, except for the well-studied 14 MeV energy region. For the ^{63}Cu(n,γ) ^{64}Cu reaction, previous data do not exist above about 3.5 MeV. This includes the 14 MeV energy region due to the competing ^{65}Cu(n,2n) ^{64}Cu reaction, which generates the same daughter nucleus, but with a three orders of magnitude higher cross section. Because of the lack of experimental data, the ENDF/B-VII.1 [5] evaluations and TENDL-2014 [6] calculations for the ^{63,65}Cu(n,γ) ^{64,66}Cu reactions differ significantly for neutron energies above 3 MeV, reaching approximately a factor of 5 at 10 MeV, while the more recent ENDF/B-VIII.b5 [5,6] evaluation is in much better agreement with the TENDL-2014 [6] calculations.

During the neutron slowing-down process, elastic and inelastic scattering are the main energy degrading processes, once the neutron energy drops below 8 MeV. In this energy region, the radiative capture and (n,α) reactions remove neutrons at the expense of producing γ rays, leptons, and α particles, which could interfere with the signals of interest in $0\nu\beta\beta$ searches. Of course, the ^{63,65}Cu(n,γ) ^{64,66}Cu cross section is much larger at thermal energies than in the energy regime studied in the present work. However, very often and depending on the detector and shielding arrangements, neutrons are captured at energies well above thermal energy; i.e., they do not reach the energy region where the capture cross section is largest. For many applications this makes no difference, but in rare decay searches like $0\nu\beta\beta$ decay, it does matter whether the daughter nucleus is excited to, say, 7.5 MeV, rather than to 10 MeV. In the latter case, the de-excitation γ-ray spectrum could contain a transition with potential interference probability, but this transition may not be present in the former case.

II. EXPERIMENTAL SETUP AND DATA-TAKING PROCEDURE

The experiment was performed at Triangle Universities Nuclear Laboratory (TUNL) [7] using the activation technique

*tornow@tunl.duke.edu

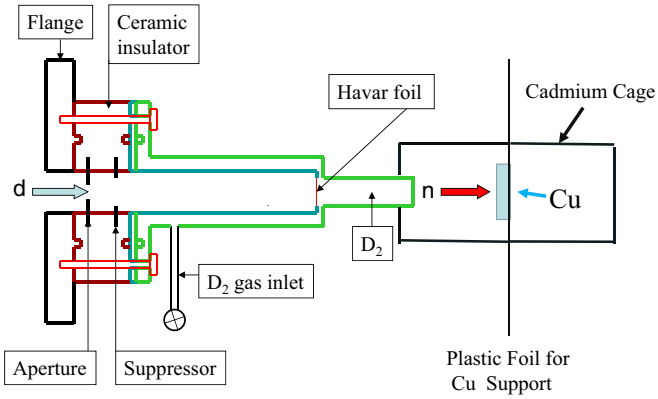

FIG. 1. Experimental setup for the ^{2}H(d,n)^{3}He neutron production reaction (not to scale). Here d stands for the incident deuteron beam, and D_2 refers to the deuterium gas.

[8,9]. Monoenergetic and quasimonoenergetic neutrons were produced via the reactions ^{3}H(p,n)^{3}He and ^{2}H(d,n)^{3}He with incident proton (p) and deuteron (d) beams, respectively. The former was used at six energies in the neutron energy range between 0.4 and 4 MeV, while the latter was employed at four energies between 4 and 7.5 MeV. The TUNL Tandem Van de Graaff accelerator provided the proton and deuteron beams, which passed through a tungsten aperture (3.5 mm wide and 4.5 mm high) before hitting the target. As shown in Fig. 1, the experimental setup for measurements with the ^{2}H(d,n)^{3}He reaction consisted of a 3-cm-long gas cell pressurized to 4 atm of high-purity deuterium gas, with a 6.5-μm-thick Havar foil separating the gas from the accelerator vacuum. According to incident neutron energies, the thickness of the 18.9-mm-diameter natural copper targets varied between 1.0 and 2.5 mm. These disks were supported by a thin plastic foil and mounted at 0° relative to the incident charged-particle beam at a distance of 2.5 cm from the end of the deuterium gas cell. To measure the neutron fluence, indium monitor foils of the same cross-sectional area and 0.125-mm thickness were attached to the front and back faces of the copper disk. The copper target and associated monitor foils were surrounded by a thin-walled cage made of cadmium (0.25-mm wall thickness) to eliminate the effect of thermal neutrons on the cross-section results. A liquid scintillator neutron detector positioned at 0° at a distance of 3 m from the deuterium gas cell was used to monitor the neutron flux. Because of the very different half-life times of the ^{64}Cu and ^{66}Cu nuclei, the ^{63}Cu(n,γ)^{64}Cu and ^{65}Cu(n,γ)^{66}Cu cross sections were measured in separate experiments.

TABLE I. Decay data for nuclear reactions used in the present work [5].

Reaction	Product half-life	E_γ (keV)	I_γ
^{63}Cu(n,γ)^{64}Cu	12.701(2) h	511.0	0.352(4)
^{65}Cu(n,γ)^{66}Cu	5.120(14) min	1039.2(2)	0.0923
^{115}In(n,n′)^{115m}In	4.486(4) h	336.24(2)	0.459(1)
^{115}In(n,γ)^{116m1}In	54.29(17) min	1293.56(2)	0.848(120)

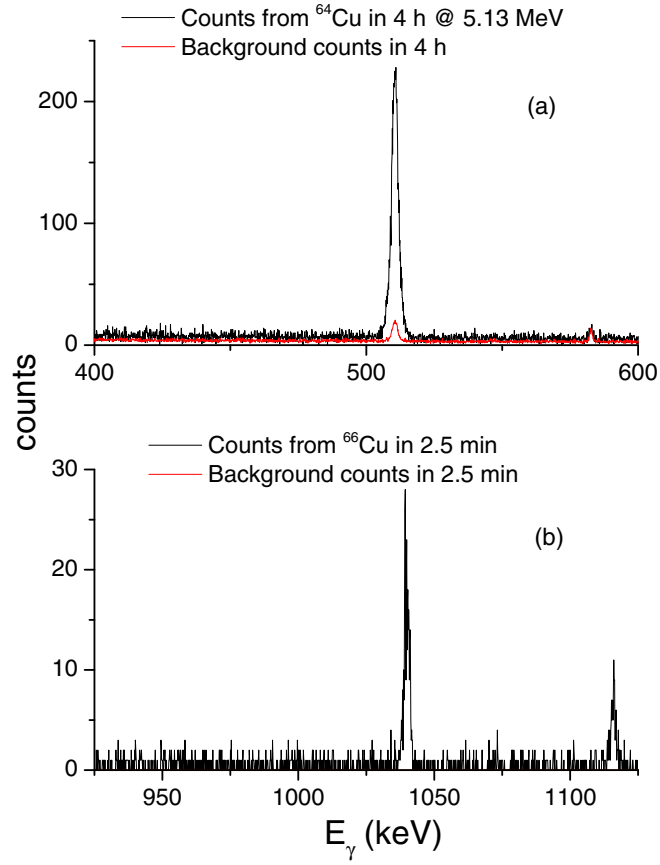

FIG. 2. Sample spectrum showing the γ-ray line of interest for incident neutron energy of 5.13 MeV for the ^{63}Cu(n,γ)^{64}Cu reaction and environmental background (a), and at 4.30 MeV for the ^{65}Cu(n,γ)^{66}Cu reaction (b).

The monoenergetic neutron beams produced by the reactions referred to above are contaminated by lower-energy neutrons once a certain charged-particle energy is exceeded. As a result, neutrons produced by the ^{3}H(d,n)^{4}He reaction with energies above 2 MeV are accompanied by lower-energy neutrons from (p,n) reactions on titanium (2.2 mg/cm^2) and the copper backing (0.4 mm) of the tritiated titanium target, which is described in Ref. [10]. To account for those unwanted neutrons, auxiliary measurements were performed with an untritiated, but otherwise identical target. Similarly, when using the ^{2}H(d,n)^{3}He reaction, low-energy neutrons are produced from the deuteron breakup on the structural material of the deuterium gas cell, once the neutron energy exceeds 5.5 MeV, which corresponds to $E_d = 2.22$ MeV. In this case, auxiliary measurements were made with the deuterium gas pumped out. The data were normalized to the integrated charge of the incident proton and deuteron beams, respectively. In the following, we will refer to these low-energy neutrons as off-energy neutrons. For the ^{2}H(d,n)^{3}He reaction, we limited the incident deuteron energy to stay below 4.45 MeV, which corresponds to $E_n = 7.8$ MeV neutron energy at 0°, to avoid deuteron breakup on the deuterium gas, because there is no easy way to correct for the associated so-called gas-breakup neutrons. After irradiation times of 15 min for the

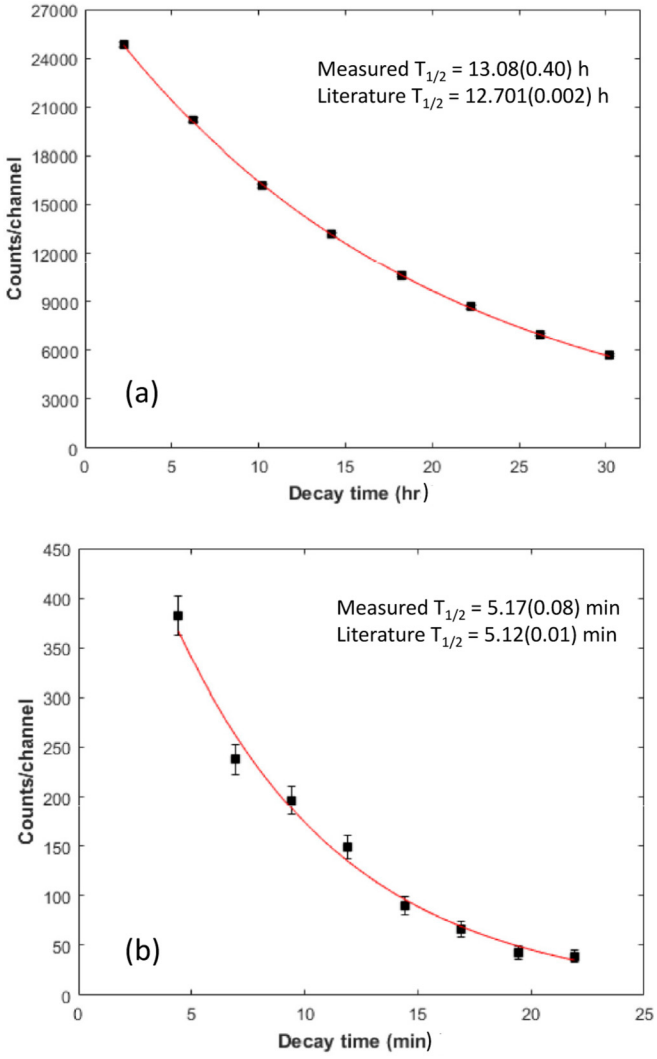

FIG. 3. Sample decay curves for the ^{63}Cu(n,γ) ^{64}Cu reaction (a), and for the ^{65}Cu(n,γ) ^{66}Cu reaction (b). In panel (a) the error bars are smaller than the symbols. The curves are least-square fits to the data.

^{65}Cu(n,γ) ^{66}Cu reaction and 45 min for the ^{63}Cu(n,γ) ^{64}Cu reaction, standard off-line γ-ray spectroscopy with well-shielded and well-characterized high-purity germanium (HPGe) detectors was used to determine the induced activities. The copper and indium foil were positioned at a distance of 5 cm from the front face of 60% and 30% relative efficiency, respectively, HPGe detectors. Table I provides relevant information on γ-ray energies, intensities, and half-life times. The abundance of ^{115}In in the natural indium foils is 95.71%. For neutron fluence determination the ^{115}In(n,γ) ^{116m}In reaction was used at E_n = 0.39 and 0.88 MeV, while the inelastic scattering reaction ^{115}In(n,n) ^{115m}In was preferred at all other neutron energies. The associated cross-section values were obtained from Refs. [11,12].

The acquired γ-ray spectra were analyzed using the TV program [13]. In Fig. 2(a) a pulse-height spectrum zoomed in on the γ-ray line of interest for the ^{63}Cu(n,γ) ^{64}Cu reaction is given. Here, the incident neutron energy is 5.13 MeV. The environmental background during the 4-h counting is

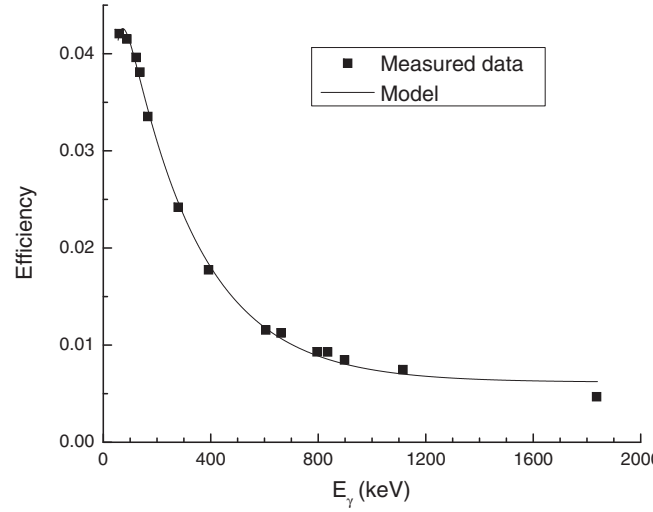

FIG. 4. Photo-peak efficiency measurements for one of the HPGe detectors used in the present work. The solid curve is a least-square fit using Eq. (1). The error bars are smaller than the symbols.

also shown for comparison. In this specific case, background measurements were done prior to irradiation to later subtract any 511 keV natural background events. Figure 2(b) presents the γ-ray line of interest for the ^{65}Cu(n,γ) ^{66}Cu reaction at 4.3 MeV. Here, the counting time is only 2.5 min. Figure 3(a) shows a typical decay curve of the 511-keV yield obtained from the ^{63}Cu(n,γ) ^{64}Cu reaction initiated with 4.3-MeV neutrons. Figure 3(b) gives a decay curve for the 1039.2-keV yield from the ^{65}Cu(n,γ) ^{66}Cu reaction, again initiated with 4.3-MeV neutrons.

In Fig. 4, data for the measured HPGe detector photo-peak efficiency are presented. They were obtained with a mixed γ-ray source containing 11 isotopes ranging from ^{241}Am (59.5 keV) to ^{88}Y (1836.1 keV). The solid curve is a least-square fit to the data using the function

$$\epsilon = p_1 + p_2\exp(-p_3E_\gamma) - p_4\exp(-p_5E_\gamma), \qquad (1)$$

from which the efficiency value can be calculated at the energies of interest.

III. DATA-ANALYSIS PROCEDURE AND RESULTS

First, the activation formula was used for the indium data for determining the neutron flux ϕ seen by the copper foils per second:

$$\phi = \frac{A\lambda}{N\sigma\epsilon I_\gamma(1-e^{-\lambda t_i})e^{-\lambda t_d}(1-e^{-\lambda t_m})}. \qquad (2)$$

Here, the induced activity A is the yield of either the 336.24- or 1293.56-keV transition from the ^{115}In reactions of interest, λ is the decay constant, N is the number of ^{115}In nuclei, σ is the ^{115}In cross section, ϵ is the photo-peak efficiency of the γ-ray transition of interest, I_γ is its intensity, t_i is the irradiation time, t_d is the decay time between the end of irradiation and the begin of the measurement, and t_m is the measurement time, with all times given in seconds.

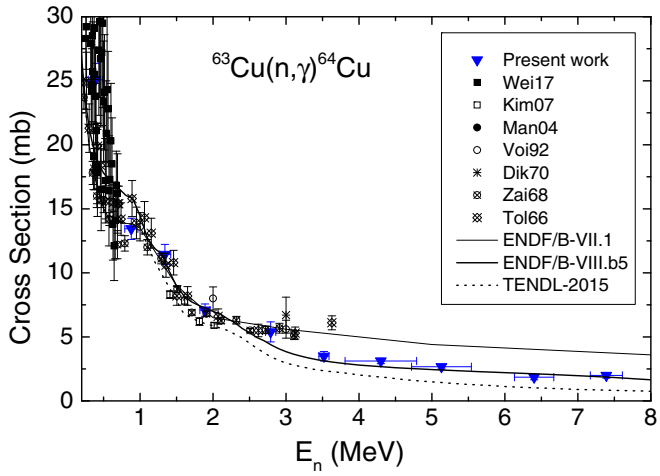

FIG. 5. Experimental results for the ^{63}Cu(n,γ) ^{64}Cu reaction cross section in comparison to the ENDF/B-VII.1 and ENDF/B-VIII.b5 evaluations and the TALYS model calculations TENDL-2015.

Next, the activation formula is used once again,

$$\sigma = \frac{A\lambda}{N\phi\epsilon I_\gamma (1 - e^{-\lambda t_i}) e^{-\lambda t_d} (1 - e^{-\lambda t_m})}, \quad (3)$$

this time with the copper data and the neutron flux determined above in order to determine the ^{63,65}Cu(n,γ) ^{64,66}Cu cross sections of interest.

Our results for the ^{63}Cu(n,γ) ^{64}Cu cross section are plotted in Fig. 5 in comparison to the previously existing data [14–19] and the ENDF/B-VII.1 and ENDF/B-VIII.b5 [5] evaluations and TENDL-2015 [6] calculation. The TENDL library is fitted to reproduce IRDF-2002 [20] instead of the more recent IRDFF [21] evaluation. As can be seen, our data agree well with the existing data in the 0.4 to 3 MeV energy range. From 3.5 to 7.5 MeV, where previous data do not exist, they follow the ENDF/B-VIII.b5 evaluation very well, while TENDL-2015 predicts smaller cross-section values. Table II (column 4) provides the data in numerical form, and Table III (column 2) details the uncertainty budget. Individual uncertainties were added in quadrature. The uncertainty in the correction factors for off-energy neutrons dominates the error budget. The correction factors are given in Table IV.

Our results for the ^{65}Cu(n,γ) ^{66}Cu reaction are shown in Fig. 6 in comparison with the previously existing data [11,17,22–26] and the ENDF/B-VII.1 and ENDF/B-VIII.b5 evaluations [5], and the TENDL-2014 [6] calculation. Our data are higher in magnitude than the previous data below $E_n = 5$ MeV but agree well with the existing data above this energy. The ENDF/B-VIII.b5 evaluation describes the previously existing data of Refs. [11,25,26] fairly well, while the TENDL-2014 calculation provides smaller cross-section values for neutron energies above 3 MeV. The previous data of Refs. [17,22–24] are not reproduced well by the ENDF/B-VIII.b5 evaluation in the 1.5 to 3.0 MeV neutron energy range. Clearly, the present data are inconsistent with the ENDF/B-VIII.b5 evaluation below 5 MeV, whereas they are in better agreement with the earlier version ENDF/B-VII.1 [5]. Our datum at 3 MeV agrees with the previous data of Colditz *et al.* [23] and Peto *et al.* [24] at this energy, but not with those of Voignier *et al.* [17] and Zaikin *et al.* [22]. In Table II (column 5), our results are tabulated, while Table III (column 3) provides details of the uncertainty budget. The off-energy neutron correction factors are given in Table V.

TABLE II. Neutron energy E_n (neutron energy spread ΔE_n is given in parenthesis), ^{115}In monitor reaction cross-section values used [11,12], and present cross-section results for ^{63}Cu(n,γ) ^{64}Cu (column 4) and ^{65}Cu(n,γ) ^{66}Cu (column 5) reactions.

E_n (MeV)	^{115}In(n,γ) ^{116m}In (mb)	^{115}In(n,n′) ^{115m}In (mb)	^{63}Cu(n,γ) ^{64}Cu (mb)	^{65}Cu(n,γ) ^{66}Cu (mb)
0.39(0.10)	176.86(3.90)		25.08(1.28)	12.53(1.30)
0.88(0.09)	150.04(5.65)		13.44(0.83)	9.03(1.12)
1.34(0.08)		137.40(3.25)	11.44(0.78)	9.65(1.10)
1.89(0.07)		246.19(5.92)	7.09(0.48)	8.59(0.97)
2.79(0.07)		343.07(8.25)	5.39(0.78)	6.60(1.10)
3.52(0.07)		334.20(7.56)	3.49(0.37)	5.03(0.89)
4.30(0.49)		315.41(7.59)	3.12(0.21)	3.44(0.25)
5.13(0.41)		332.25(8.62)	2.67(0.18)	2.55(0.29)
6.40(0.27)		344.05(12.73)	1.85(0.20)	1.67(0.67)
7.39(0.22)		319.34(10.88)	1.99(0.21)	1.82(0.70)

TABLE III. Uncertainty budget for ^{115}In monitor, ^{63}Cu(n,γ) ^{64}Cu, and ^{65}Cu(n,γ) ^{66}Cu reaction cross-section values.

Uncertainty	^{115}In (%)	^{63}Cu (%)	^{65}Cu (%)
Counting statistics	0.1–1.4	0.8–1.6	2.5–3.6
Reference cross sections	2.2–3.4		
HPGe detector efficiency	3–5	3	4
Source geometry and self-absorption of γ rays	<1	<1.4	<1.7
γ-ray intensity	1.4	1.1	1.1
Neutron flux fluctuation correction	<1	<1	<1
Off-energy neutron correction factor	<10	<13	<18

IV. SUMMARY

In summary, the present work provides the first neutron radiative capture data on the nuclei ^{63}Cu and ^{65}Cu in the neutron energy range between 4 and 7.5 MeV and supplements

TABLE IV. Percentage contribution of off-energy neutron induced activity for ^{63}Cu(n,γ) ^{64}Cu measurements in In monitor foils and Cu targets. At the other energies studied in the present work, the correction factors were negligible.

E_n (MeV)	In correction factor (%)	^{64}Cu correction factor (%)
2.79	2.7	24.4
3.52	10.1	63.0
6.40	1.5	14.0
7.39	2.5	12.6

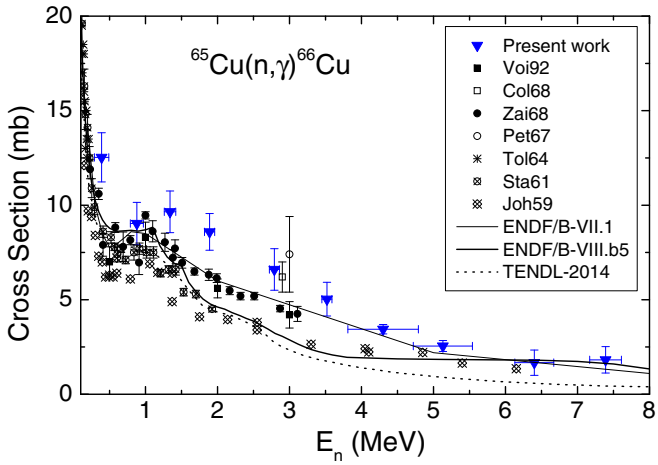

FIG. 6. Experimental results for the ^{65}Cu(n,γ) ^{66}Cu reaction cross section in comparison to the ENDF/B-VII.1 and ENDF/B-VIII.b5 evaluations and the TALYS model calculations TENDL-2014.

existing data between 0.4 to 4 MeV. The new data are important to guide evaluations and model calculations at higher energies. The data are needed to improve our knowledge about potential neutron-induced background contributions in the energy windows of importance for $0\nu\beta\beta$ decay searches.

TABLE V. Percentage contribution of off-energy neutron induced activity for ^{65}Cu(n,γ) ^{66}Cu measurements in In monitor foils and Cu targets. At the other energies studied in the present work, the correction factors were negligible.

E_n (MeV)	In correction factor (%)	^{66}Cu correction factor (%)
2.79	1.2	15.0
3.52	8.4	41.2
6.40	1.3	11.7
7.39	2.6	13.3

ACKNOWLEDGMENTS

This work was supported in part by the United States Department of Energy, Office of Nuclear Physics, under Grant No. DE-FG02-97ER41033. I.N. acknowledges support from the National Science Foundation through the 2015 REU Grant No. NSF-PHY-1461204 to TUNL. The authors thank S. W. Finch for valuable contributions.

[1] J. Albert *et al.* (EXO-200 Collaboration), Nature **510**, 229 (2014).
[2] A. Branca *et al.* (CUORE Collaboration), arXiv:1705.00005v2 (2016); C. Alduino *et al.* (CUORE Collaboration), Phys. Rev. Lett. **120**, 132501 (2018).
[3] M. Agostini *et al.* (GERDA Collaboration), Nature **544**, 47 (2017).
[4] M. Abgrall *et al.*, Adv. High Energy Phys. **2014**, 1 (2014).
[5] http://www.nndc.bnl.gov.
[6] http://www-nds.indcentre.org.in/exfor/endf.htm.
[7] http://www.tunl.duke.edu.
[8] M. Bhike, B. Fallin, M. E. Gooden, N. Ludin, and W. Tornow, Phys. Rev. C **91**, 011601(R) (2015).
[9] Krishichayan, M. Bhike, W. Tornow, A. P. Tonchev, and T. Kawano, Phys. Rev. C **96**, 044623 (2017).
[10] M. Bhike, B. Fallin, and W. Tornow, Phys. Lett. B **736**, 361 (2014).
[11] A. E. Johnsrud, M. G. Silbert, and H. H. Barschall, Phys. Rev. **116**, 927 (1959).
[12] A. B. Smith, S. Chiba, D. L. Smith, J. W. Meadows, P. T. Guenther, R. D. Lawson, and R. J. Howerton, ANL/NDM-115 (1990), http://www.ne.anl.gov/capabilities/nd/reports/ANLNDM-115.pdf.
[13] J. Theuerkauf, S. Esser, S. Krink, M. Luig, N. Nicolay, O. Stauch, and H. Wolters, Program TV, Institute of Nuclear Physics, University of Cologne, 1993 (unpublished).
[14] M. Weigand, C. Beinrucker, A. Couture, S. Fiebiger, M. Fonseca, K. Göbel, M. Heftrich, T. Heftrich, M. Jandel, F. Käppeler, A. Krása, C. Lederer, H. Y. Lee, R. Plag, A. Plompen, R. Reifarth, S. Schmidt, K. Sonnabend, and J. L. Ullmann, Phys. Rev. C **95**, 015808 (2017).
[15] G. D. Kim, H. J. Woo, H. W. Choi, N. B. Kim, T. K. Yang, J. H. Chang, and K. S. Park, J. Radiol. Nucl. Chem. **271**, 553 (2007).
[16] W. Mannhart and D. Schmidt, AIP Conf. Proc. **769**, 609 (2005).
[17] J. Voignier, S. Joly, and G. Grenier, J. Nucl. Sci. Eng. **112**, 87 (1992).
[18] M. Diksic, P. Strohal, G. Peto, P. Bornemisza-Pauspertl, I. Hunyadi, and J. Karolyi, Acta Physica Hungarica **28**, 257 (1970).
[19] V. A. Tolstikov, V. P. Koroleva, V. E. Kolesov, and A. G. Dovbenko, Atomnaya Energiya **21**, 45 (1966).
[20] https://www-nds.iaea.org/irdf2002/index.htmlx.
[21] https://www-nds.iaea.org/IRDFF/.
[22] G. G. Zaikin, I. A. Korzh, N. T. Sklyar, and I. A. Totskii, Sov. At. Energy **25**, 1362 (1968).
[23] J. Colditz and P. Hille, J. Oesterr. Akad. Wiss., Math, -Naturw. KI Anzeiger **105**, 236 (1968).
[24] G. Peto, Z. Milligy, and I. Hunyadi, J. Nucl. Energy **21**, 797 (1967).
[25] V. A. Tolstikov, V. E. Kolesov, A. G. Dovbenko, and Ju. Ja. Stavisskij, Atomnaya Energiya **17**, 505 (1964).
[26] Ju. Ya. Stavisskiy and V. A. Tolstikov, Atomnaya Energiya **10**, 508 (1961).